



Transport Properties of Mixtures of Acid Gases with Aqueous Monoethanolamine Solutions: A Molecular Dynamics Study

H. Mert Polat, Frédérick de Meyer, Houriez Céline, Christophe Coquelet, Othonas Moulτος, Thijs J.H. Vlugt

► To cite this version:

H. Mert Polat, Frédérick de Meyer, Houriez Céline, Christophe Coquelet, Othonas Moulτος, et al.. Transport Properties of Mixtures of Acid Gases with Aqueous Monoethanolamine Solutions: A Molecular Dynamics Study. *Fluid Phase Equilibria*, 2023, 564, pp.113587. 10.1016/j.fluid.2022.113587 . hal-03784182

HAL Id: hal-03784182

<https://hal.science/hal-03784182>

Submitted on 22 Sep 2022

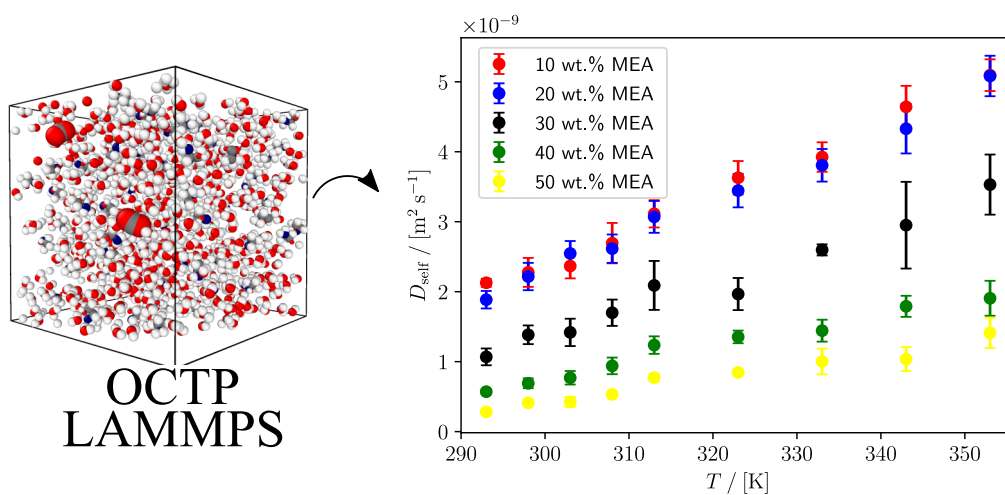
HAL is a multi-disciplinary open access archive for the deposit and dissemination of scientific research documents, whether they are published or not. The documents may come from teaching and research institutions in France or abroad, or from public or private research centers.

L'archive ouverte pluridisciplinaire **HAL**, est destinée au dépôt et à la diffusion de documents scientifiques de niveau recherche, publiés ou non, émanant des établissements d'enseignement et de recherche français ou étrangers, des laboratoires publics ou privés.

Graphical Abstract

Transport Properties of Mixtures of Acid Gases with Aqueous Monoethanolamine Solutions: A Molecular Dynamics Study

H. Mert Polat, Frédéric de Meyer, Céline Houriez, Christophe Coquelet, Othonas A. Moulton, Thijs J. H. Vlugt



Transport Properties of Mixtures of Acid Gases with Aqueous Monoethanolamine Solutions: A Molecular Dynamics Study

H. Mert Polat^{a,b,c}, Frédéric de Meyer^{a,b}, Céline Houriez^b, Christophe Coquelet^b, Othonas A. Moultos^c, Thijs J. H. Vlugt^{c,*}

^a*CCUS R&D Program, Gas & Low Carbon Entity, OneTech, TotalEnergies S.E., 92078 Paris, France*

^b*CTP - Centre of Thermodynamics of Processes, Mines ParisTech, PSL University, 35 rue Saint Honoré, 77305 Fontainebleau, France*

^c*Engineering Thermodynamics, Process & Energy Department, Faculty of Mechanical, Maritime and Materials Engineering, Delft University of Technology, Leeghwaterstraat 39, Delft 2628CB, The Netherlands*

Abstract

We investigated the effect of temperature and monoethanolamine (MEA) concentration on the self-diffusivity of acid gases, CO₂, and H₂S in aqueous MEA solutions. For this purpose, we computed densities of pure MEA and 30 wt.% MEA/water solutions while scaling the LJ energy (ϵ) parameter and point charges of MEA. Results show that with a scaling factor of 0.80 applied to the point charges of MEA, computed densities agree well with the experimental ones from literature. This was tested by computing viscosities and the self-diffusivity of pure MEA and 30 wt.% MEA/water solutions and comparing these with experiments. We showed that the scaling factor of 0.80 also works well for predicting transport properties of MEA/water solutions. Finally, we computed self-diffusivities of infinitely diluted CO₂ and H₂S for temperatures ranging from 293–353 K and MEA concentrations of 10–50 wt.%. Our results show that the self-diffusivity of both acid gases depends significantly on the temperature and MEA concentration in the solution. The results of this study will contribute to the development of more efficient acid gas treatment processes.

*Corresponding author

Email address: t.j.h.vlugt@tudelft.nl (Thijs J. H. Vlugt)

Keywords: Molecular simulation, Carbon dioxide, Hydrogen sulfide, Transport properties, Diffusion

1. Introduction

Natural gas is the fossil fuel with the highest energy density per carbon atom [1]. NO_x and particulate matter emissions from the process of natural gas burning are lower compared to other fossil fuels [2]. Natural gas will play a key role in hydrogen production [3]. These advantages make natural gas a promising candidate to replace liquid fossil fuels and coal, and to be a transition fuel until renewable energy sources are feasible on a large scale [4, 5]. It is well known that about 40% of the remaining natural gas sources have a CO_2 concentration higher than 2% and a H_2S concentration higher than 100 ppm [6]. The acid gas concentration in natural gas needs to be reduced to <2% and <50 ppm of CO_2 for pipeline and liquefied natural gas (LNG) transport, respectively, and <4 ppm of H_2S for both pipeline gas and LNG [6]. The removal of acid gases from natural gas streams can be achieved by several different processes such as adsorption-based separation [7], membrane separation [8], cryogenic distillation [9], direct conversion of H_2S to elemental sulfur [10] and, absorption-based separation using liquid solvents. The latter option is widely preferred since it is a technically mature, and a reliable process, and it offers a low amount of absorbed hydrocarbons [11].

In absorption-based separation processes, CO_2 and H_2S are removed by a liquid solvent, usually aqueous alkanolamines, by physical and/or chemical absorption [12, 13, 14, 15]. In this process, a natural gas stream flows through the absorption column at high pressure (20–100 bar) and mild temperature (313–353 K) and acid gases are absorbed into the liquid solvent [16]. After absorption, the liquid solvent is sent to the regeneration column where it is regenerated at high temperature (typically 363–383 K). This process can be optimized using process simulation software [17] in which the diffusion coefficients of the acid gases inside the liquid phase are used to simulate the reaction kinetics [11]. Since both CO_2 and H_2S react with the solvent, it is experimentally not possible to directly measure their diffusion coefficients. Instead, the experimental studies measure the diffusion coefficient of non-reacting model molecules [18], such as N_2O to replace CO_2 , and calculate the diffusion coefficient of the required acid gas from the diffusion coefficient

of the model molecule [19, 20, 21]. Sada et al. [22] measured the diffusion coefficients of N_2O in aqueous solutions of five different amines including monoethanolamine (MEA) at 298 K and calculated the diffusion coefficient of CO_2 using the diffusion coefficients of N_2O . Ko et al. [23] measured N_2O absorption rates in aqueous solutions of various amines at 303, 308 and 313 K and calculated the diffusion coefficients using the absorption rates. Ying and Eimer [24] also measured the diffusion coefficients of N_2O in aqueous MEA solutions for a temperature range between 298 K and 333 K and calculated the diffusion coefficients of CO_2 using the $\text{CO}_2/\text{N}_2\text{O}$ analogy [19].

Force field-based molecular dynamics (MD) simulations have been extensively used to predict diffusion coefficients of different solutes such as alkylbenzenes, ketones, and water in various solvents [25, 26]. This simulation method requires an accurate description of the interaction between the molecules of the solute and the solvent i.e., interaction potentials that describe the interactions between the molecules accurately. The advantage of MD simulations is that reactions in the system can be “switched off”, eliminating the need for a model molecule in the experimental studies. Although MD simulations have been very promising and are widely used for this purpose [20, 15], we currently have limited knowledge of the diffusion coefficients of CO_2 and H_2S and their temperature dependence in solutions with different concentrations of alkanolamine in the solvent. The diffusivity of acid gases in pure water has been studied extensively [27, 28, 29]. Only two simulation studies in the literature report diffusion coefficients of acid gases in aqueous MEA solutions. To validate the $\text{CO}_2/\text{N}_2\text{O}$ analogy, Chen et al. [20] have computed the self-diffusivities of CO_2 and N_2O in aqueous MEA solution at 303 K. Melnikov and Stein [30] have computed the diffusion coefficient of CO_2 in aqueous MEA solution as a function of CO_2 loading at 313 K. This study revealed that the diffusion coefficients of all the species in CO_2 loaded aqueous MEA solution decrease significantly with increasing CO_2 loading.

In this study, we compute self-diffusion coefficients (D_{self}) for CO_2 and H_2S in aqueous MEA solutions for a wide range of temperatures and MEA concentrations in the solution. We studied aqueous MEA solutions because it is considered as an industry benchmark solvent [31] and it is also used for CO_2 capture from flue gas [32]. We first computed the density of pure MEA solution for the temperature range 293–353 K. It turns out that with the standard force fields from literature, the results did not agree with the experimental density values from literature. We then scaled the force field parameters of MEA molecules to find the optimum scaling factor that best

describes the experimental densities of the solvent. We validated this set of parameters by calculating the viscosities and D_{self} of pure MEA and 30 wt.% MEA/water solution and compared these values to experimental values from literature. We used the validated force field for MEA to compute the self-diffusivities of CO_2 and H_2S at infinite dilution for a temperature range of 293–353 K and MEA concentrations ranging from 10–50 wt.% in the solvent. The results we provide will be useful for more accurate modelling in the process simulations, and will guide the design and development of acid gas removal process.

This article is organized as follows: the force field parameters and the simulation methods are discussed in the next section. In section 3, we discuss the results from the simulations and compare them with available literature data. In the final section, we provide conclusions regarding to the diffusivity of acid gases in aqueous MEA solutions.

2. Simulation Methods

Monte Carlo (MC) simulations to compute solvent densities were performed using the open source MC software, Brick-CFCMC [33, 34, 35]. For MEA molecules, the OPLS-AA [36, 37] force field was used for intermolecular Lennard-Jones (LJ) interactions because it was optimized for amines. Partial charges computed from quantum mechanical calculations were used for electrostatic interactions of MEA molecules. Quantum chemical calculations were performed using the Gaussian09 [38] software at second order Møller-Plesset perturbation theory (MP2) [39] level using the 6-311+G(2d,2p) basis set. **We then multiply either the energy (ϵ) parameters of LJ interactions of MEA molecule or the point charges of MEA molecule with a scaling factor χ to scale the interactions of this molecule.** For water molecules, the SPC/E [40] force field was used. The SPC/E force field is known to predict the transport properties of water accurately [41]. **For CO_2 molecules, the TraPPE [42] force field was used. The interactions between the TraPPE CO_2 molecules and the SPC/E water molecules were computed using the optimized intermolecular potential for $\text{CO}_2/\text{H}_2\text{O}$ developed by Orozco et al. [43]. For H_2S molecules, the force field developed by Kristóf and Liszi [44] were used.** All force field parameters for these molecules can be found in the Supporting Information (Tables S1-S3). LJ parameters of the interactions of different types of atoms **except the interactions between CO_2 and water molecules [43]** were computed using Lorentz-Berthelot mixing rules [45]. All molecules in

the molecular simulations were kept rigid. It was shown that the rigidity of small molecules (length of MEA molecule ≈ 3 Å) does not significantly affect the dynamics in MD simulations [45]. Initial configurations were generated in a cubic simulation box with a length of 25.5 Å using Packmol [46]. For initialization, equilibration and production stages, 10^4 , 10^5 and 10^5 MC cycles were performed, respectively. In MC cycles, the number of trial moves is equal to the number of molecules in the simulation box. These moves were the translation of a randomly selected molecule (49.5%), the rotation of a randomly selected molecule (49.5%) and attempting to change the volume of the simulation box (1%). In these simulations, LJ interactions were truncated at 12 Å and analytic tail corrections [45] were applied. To compute the electrostatic interactions, the Ewald summation [47] was used with a precision of 10^{-6} . Standard deviations for densities of pure MEA and 30 wt.% MEA/water solutions were computed using block averaging over the densities computed in the production stage of the MC simulations.

Initial configurations for the MD simulations were generated with a box length of 50 Å using Packmol [46]. The number of MEA and water molecules used for different concentrations of MEA in the solution are listed in Table 1. Two molecules of CO_2 or H_2S were used to compute the self-diffusivity of these species. The MD simulations start with an equilibration period of 0.5 ns with a timestep of 1 fs in the *NPT* ensemble using the Nosé-Hoover thermostat and barostat. After this equilibration, the temperature was equilibrated in the *NVT* ensemble using the Nosé-Hoover thermostat for another 0.5 ns. In the production stage, the simulations were run for 100 ns in the *NVE* ensemble with a timestep of 1 fs. In these simulations, LJ interactions were truncated at 12 Å. Analytic tail corrections [45] were applied to account for the long-range interactions. Electrostatic interactions were computed using the Particle-Particle Particle-Mesh (PPPM) method with a relative precision of 10^{-5} . MD simulations to compute viscosities and self-diffusivities were performed using the LAMMPS [48] package (version 3 March 2020) with the OCTP [49] plugin. The computed self-diffusion coefficients were corrected for the finite-size effects [50, 51, 52]. It is important to note that the computed self-diffusion coefficients of the acid gases are practically equal to transport diffusion coefficients because the acid gases are at low loading [53]. The standard deviations of the self-diffusion coefficients and the viscosities were computed from ten independent simulations starting from different initial configurations. **The radial distribution functions (RDFs) computed in this study are center-of-mass radial distribution functions.**

Table 1: Number of MEA and water molecules in MD simulations for different concentrations of MEA in the MEA/water solutions.

MEA concentration / [wt.%]	Number of MEA molecules	Number of water molecules	Average Box Size at 313 K / [Å]
10	25	775	29.1
20	55	745	29.8
30	81	646	29.9
40	123	627	30.5
50	159	541	30.8

3. Results and Discussion

LJ interaction parameters for MEA were taken from the OPLS-AA force field [36, 37]. The point charges of MEA were computed using quantum chemical calculations as discussed in the previous section. Generic force fields such as OPLS-AA and point charges calculated using quantum chemical calculations may require scaling (with different methods) [54, 55, 56, 57, 58, 59]. The reason for this is that point charges calculated using quantum chemical calculations typically overestimate electrostatic interactions [54, 57, 60, 61, 62, 58]. To test the performance of the force field for MEA, we first calculated the density of a pure MEA solution and a 30 wt.% MEA/water solution for a temperature range of 293–353 K using MC simulations. Comparison between computed and experimental densities [63, 64, 65] are shown in Fig. 1. Results showed that computed densities using this force field do not agree well with experimental measurements [63, 64, 65]. This is because strong polarization and charge transfer in these solutions are not well produced by this force field [55]. We scaled the energy (ϵ) parameter of the LJ potential and the point charges of the MEA molecule by multiplying either ϵ or the point charges with a scaling factor, χ . Fig. 1 shows the densities of pure MEA solvent and 30 wt.% MEA/water solution as a function of temperature and χ . Results show that changing the LJ potential does not affect the densities of both pure MEA and 30 wt.% MEA/water solution significantly, while scaling the point charges significantly affects the density of these solutions. Figure S1 of the Supplementary Material shows that scaling the LJ ϵ parameter of the MEA atoms by $\chi = 0.7$ changes the density of pure MEA solution (30 wt.%

MEA/water solution) by ca. 0.4% (1.1%) at 303 K. The scaling of the point charges of MEA by the same χ changes the density of pure MEA by ca 10% and the density of 30 wt.% MEA/water solution by ca. 4% (Fig. 1(b) and (d)). Overall, these results suggest that calculated densities of pure MEA and 30 wt.% MEA/water solutions agree well with the experimental values when the point charges of MEA are scaled by 0.8, with a maximum deviation of ca. 3% from experiments for both solutions (Fig. 1 (b) and (d)).

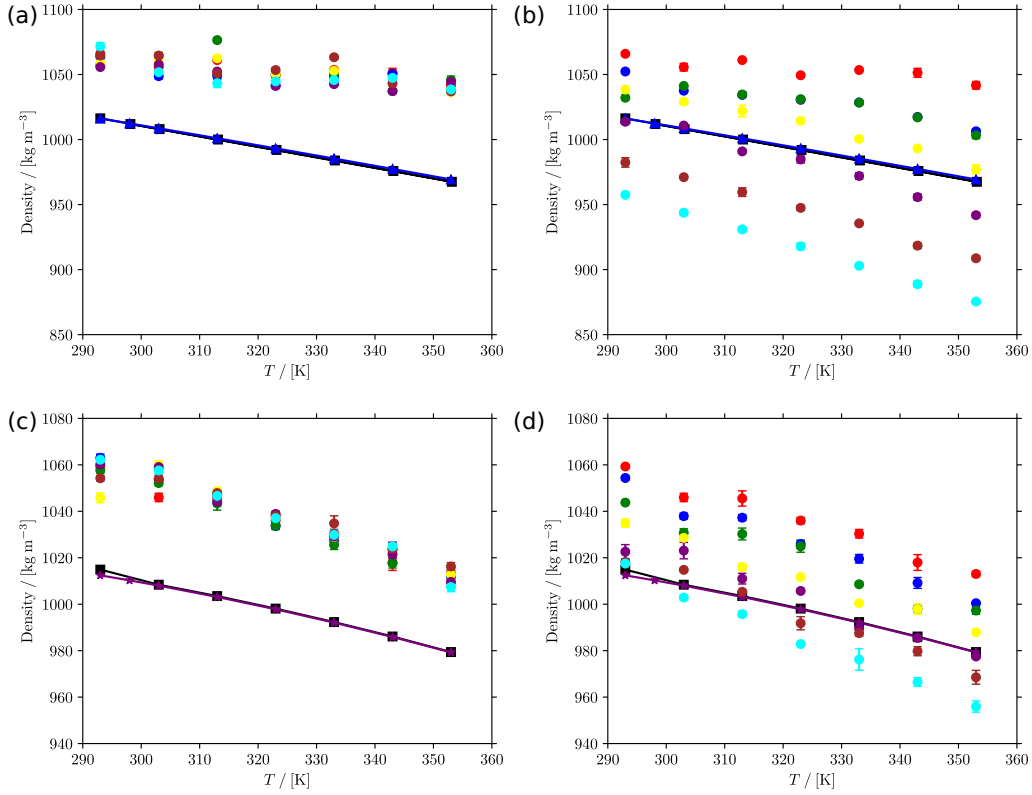


Figure 1: Comparison of simulated and experimental [63, 64, 65] densities of (a,b) pure MEA and (c,d) 30 wt.% MEA/water solutions as a function of temperature. Subfigures (a) and (c) show the scaling of LJ ϵ parameters of the MEA molecules while subfigures (b) and (d) show the scaling of the point charges of the MEA molecules. Red: $\chi = 1.00$; blue: $\chi = 0.95$; green: $\chi = 0.90$; yellow: $\chi = 0.85$; purple: $\chi = 0.80$; brown: $\chi = 0.75$; cyan: $\chi = 0.70$; black: experimental [63], blue: experimental correlation [64, 65]. The lines connecting the experimental data are to guide the eye.

Motivated by the good agreement between simulations and experiments on the densities of pure MEA and 30 wt.% MEA/water solutions, we validated the scaling factor for the point charges, i.e. $\chi = 0.80$, of MEA by computing the viscosities and D_{self} of these solutions using MD simulations for a temperature range of 293–353 K. We have used 30 wt.% MEA/water solution to validate our model for MEA because this is the most studied solution in literature and the industry standard for CO₂ capture [66]. It is important to note that we scaled the point charges of MEA with $\chi = 0.8$ in these simulations. Fig. 2 shows the comparison between the computed and experimental [63] viscosities and D_{self} of pure MEA and 30 wt.% MEA/water solutions. Results show that the computed and experimental viscosities of pure MEA and 30 wt.% MEA/water solutions have coefficient of determination (R^2) [67] scores of 0.98 and 0.97, respectively. Both R^2 scores show that the simulations, and therefore this set of force field parameters for MEA, agree well with the experiments on viscosity in this temperature range. We also compare the simulation results with the experimental correlation obtained from Design Institute for Physical Properties (DIPPR) [64] (Fig. 2(a)). The simulations agree well also with the experimental correlation obtained from the DIPPR database. For example, the computed viscosities for pure MEA (30 wt.% MEA/water) were between 26.26–2.42 (2.69–0.91) mPa · s at 293–353 K. The experimental values for the same conditions vary between 24.09–2.92 and 2.91–0.77 mPa · s for pure MEA and 30 wt.% MEA/water solutions, respectively. The maximum (average) deviation between computed viscosities and experimental viscosities were computed as 17% (8.8%) and 15% (7.6%) for pure MEA and 30 wt.% MEA/water solutions, respectively. These results suggest that using the scaling factor ($\chi = 0.8$) for the point charges of MEA in these simulations can provide accurate predictions for the viscosity of MEA/water solutions. We also compared the computed D_{self} (corrected for finite-size effects using computed viscosities [50, 51]) of MEA molecules in pure MEA solution with the experimental values from literature [68]. The experimental values are $4.2 \times 10^{-11} \text{ m}^2 \text{ s}^{-1}$, $5.5 \times 10^{-11} \text{ m}^2 \text{ s}^{-1}$, and $9.3 \times 10^{-11} \text{ m}^2 \text{ s}^{-1}$ for 288, 298, and 308 K, while the computed D_{self} are $4.5 \times 10^{-11} \text{ m}^2 \text{ s}^{-1}$ (extrapolated slightly using an Arrhenius equation fit, R^2 for Arrhenius fit = 0.997), $5.6 \times 10^{-11} \text{ m}^2 \text{ s}^{-1}$, and $1.1 \times 10^{-10} \text{ m}^2 \text{ s}^{-1}$, respectively. To the best of our knowledge, there is no experimental data in literature to compare D_{self} of water and MEA molecules in 30 wt.% MEA/water solutions. The value of D_{self} of water molecules is 2.14–2.34 times larger than the MEA molecules in 30 wt.% MEA/water solutions. Also, the results show that the self diffusivity D_{self} of MEA is an

order of magnitude higher in 30 wt.% MEA/water solution than that in a pure MEA solution. This indicates stronger MEA-MEA interactions than MEA-water interactions.

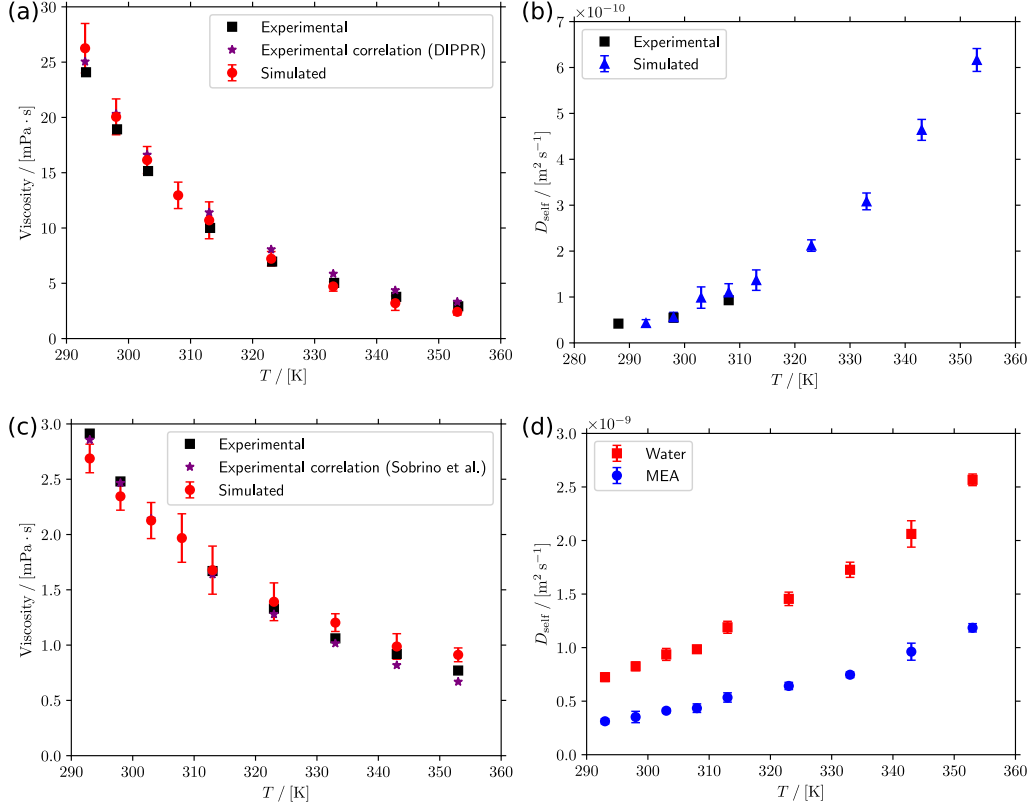


Figure 2: Comparison of simulated and experimental [63, 64, 65, 69] viscosities of (a) pure MEA and (c) 30 wt.% MEA/water solution as a function of temperature. D_{self} of (b) MEA molecules in pure MEA and (d) MEA and water molecules in 30 wt.% MEA/water solution as a function of temperature.

To obtain a fundamental understanding of the transport mechanism of CO_2 and H_2S in MEA/water solutions with different MEA concentrations, we computed D_{self} of CO_2 , H_2S , **water, and MEA molecules** in 10–50 wt.% MEA/water solutions at infinite dilution and 1 bar for a temperature range of 293–353 K using MD simulations. Fig. 3 shows D_{self} of both acid gases in pure water [27, 28] and 10–50 wt.% MEA/water solutions as a function of temperature and MEA concentration. **Fig S3. shows computed viscosities of aqueous MEA solutions as a function of temperature and MEA concentration.** Fig. S4 shows D_{self} of water and MEA molecules as a function of temperature and MEA concentration. We first compare computed values of D_{self} of CO_2 with values of D_{self} of CO_2 obtained using $\text{CO}_2/\text{N}_2\text{O}$ analogy [70]. Mandal et al. [70] estimated values of D_{self} of CO_2 in 30 wt.% MEA/water solution as $1.61 \times 10^{-9} \text{ m}^2 \text{ s}^{-1}$, $1.74 \times 10^{-9} \text{ m}^2 \text{ s}^{-1}$, and $2.14 \times 10^{-9} \text{ m}^2 \text{ s}^{-1}$ at 293 K, 303 K, and 313 K, respectively. The values of D_{self} of CO_2 we computed in 30 wt.% MEA/water solution are $1.1 \times 10^{-9} \text{ m}^2 \text{ s}^{-1}$, $1.4 \times 10^{-9} \text{ m}^2 \text{ s}^{-1}$, and $2.1 \times 10^{-9} \text{ m}^2 \text{ s}^{-1}$ at 293 K, 303 K, and 313 K, respectively. These results show that simulated values of D_{self} of CO_2 are slightly underestimated for the temperatures 293 K and 303 K while at 313 K the computed value of D_{self} of CO_2 agrees with the value obtained using $\text{CO}_2/\text{N}_2\text{O}$ analogy [70].

Our results show that D_{self} of both acid gases increase with increasing temperature. Fig. 3 also shows that D_{self} of CO_2 is larger than D_{self} of H_2S at the same conditions. Although H_2S has a lower molar mass ($M_{\text{H}_2\text{S}} = 34.1 \text{ g mol}^{-1}$) than CO_2 ($M_{\text{CO}_2} = 44.01 \text{ g mol}^{-1}$), its values of D_{self} is lower because it can form hydrogen bonds with both water and MEA molecules, and the H_2S molecule is more spherical than the linear CO_2 molecule [71]. Also, the results show that with the increasing concentration of MEA in the solution both D_{self} of CO_2 and H_2S in these solutions decrease. For CO_2 (H_2S), D_{self} at 293 K decreases by a factor of 7.6 (6.8) times from 10 wt.% MEA to 50 wt.% MEA while at 353 K, D_{self} decrease by a factor of 3.6 (3.4) times. The temperature dependency of the D_{self} of both CO_2 and H_2S decreases with increasing MEA concentration in the solution. **The same temperature dependency can also be observed in D_{self} of water and MEA molecules (Fig. S4).** The slope of D_{self} as a function of temperature in a 10 wt.% solution is 3.0 and 2.7 times higher than 50 wt.% solution for CO_2 and H_2S , respectively. Also, D_{self} changes significantly for both acid gases from 40 wt.% solution to 30 wt.%, especially at low temperatures. However, the changes in D_{self} of both acid gases are not as significant from 50 wt.% to 40 wt.%. For example, D_{self} of H_2S at 293 K increases by 2.2 times from 40 wt.%

solution to 30 wt.% solution while it only increases by a factor of 1.7 from 50 wt.% to 40 wt.%. This effect of MEA concentration on D_{self} decreases with the increasing temperature as D_{self} of H_2S increases 1.5 times both from 40 wt.% to 30 wt.% and from 50 wt.% to 40 wt.% at 353 K. For CO_2 , **water and MEA**, there is also a significant effect of concentration on D_{self} from 30 wt.% MEA/water solution to 20 wt.% MEA/water solution (**Fig. 3(a) and Fig. S4**). We fit the value of D_{self} of CO_2 and H_2S to an Arrhenius equation using:

$$D_{\text{self}} = D_0 \exp \left[-\frac{E_A}{RT} \right] \quad (1)$$

where D_0 is the pre-exponential factor, E_A is the activation energy for diffusion, R is the ideal gas constant, and T is the absolute temperature. Fig. 3(b,d) shows the Arrhenius fits for D_{self} of CO_2 and H_2S . Tables 2 and 3 shows Arrhenius fit parameters for D_{self} of CO_2 and H_2S . **Tables 2 and 3 show that the activation energy for diffusion for both acid gases increase with increasing MEA concentration in the solution. This was also indicated by slower acid gas dynamics (Fig. 3) with increasing MEA concentration.** We also fit the D_{self} of CO_2 and H_2S to the Speedy-Angell power equation [72] (**Eq. S1**) and the Vogel-Tamann-Fulcher (VTF) equation [73] (**Eq. S2**). Tables S8-11 of the Supplementary Material show the Speedy-Angell power equation and the VTF equation fit parameters for CO_2 and H_2S . Figure S2 of the Supplementary Material shows the Speedy-Angell and VTF fits for D_{self} of CO_2 and H_2S in aqueous MEA solutions. The pressure and temperature dependent form of the Speedy-Angell power equation has been shown to be able to predict the CO_2 diffusivity in water very accurately [29]. Our results show that the Speedy-Angell power equation has the highest coefficients of determination (R^2) for D_{self} of CO_2 and H_2S between the Arrhenius equation, the Speedy-Angell power equation and the VTF equation.

We performed two more sets of MD simulations to measure the sensitivity of values of D_{self} of acid gases with respect to the point charge scaling factor χ . We computed values of D_{self} of CO_2 as $3.48_{0.3} \times 10^{-9} \text{ m}^2 \text{ s}^{-1}$, $3.53_{0.4} \times 10^{-9} \text{ m}^2 \text{ s}^{-1}$, and $2.66_{0.2} \times 10^{-9} \text{ m}^2 \text{ s}^{-1}$ for $\chi = 0.7$, $\chi = 0.8$, and $\chi = 1.0$, respectively, at 353 K and 1 bar in 30 wt.% MEA/water solution. This shows that the value of D_{self} of CO_2 change significantly with the scaling from $\chi = 1.0$ to $\chi = 0.8$ while the change in the value of D_{self} of CO_2 from $\chi = 0.8$ to $\chi = 0.7$ is not significant (within the error bars shown as subscripts in this paragraph).

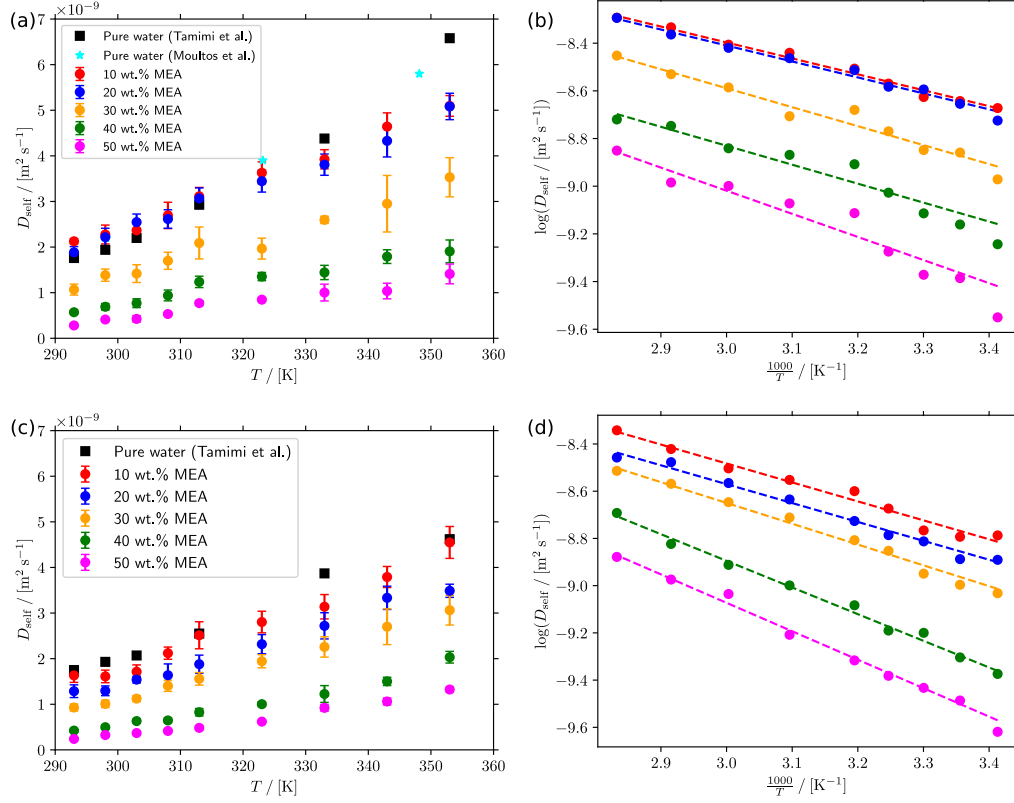


Figure 3: Self-diffusion coefficients of (a) CO_2 and (c) H_2S in pure water [27, 28] and 10–50 wt.% MEA/water solutions as a function of temperature. Subfigures (b) and (d) show the Arrhenius plots of subfigures (a) and (c), respectively. In subfigures (b) and (d), color codes follow those in subfigures (a) and (c). Dashed lines represent the Arrhenius fits of the D_{self} . The Speedy-Angell [72] and the VTF [73] equation fits are shown in Figure S2 of the Supplementary Material.

Table 2: Arrhenius fit parameters (pre-exponential factor (D_0) and activation energy (E_A)) and coefficient of determinations (R^2) for D_{self} of CO_2 in MEA/water solutions with different MEA concentrations. The values of D_{self} of CO_2 were fitted for a temperature range of 293–353 K.

MEA concentration / [wt. %]	D_0 / [$\text{m}^2 \text{s}^{-1}$]	E_A / [kJ mol^{-1}]	R^2
10	4.05×10^{-7}	12.79	0.989
20	3.98×10^{-7}	12.82	0.988
30	6.28×10^{-7}	15.23	0.970
40	3.59×10^{-7}	15.23	0.947
50	7.77×10^{-7}	18.57	0.944

Table 3: Arrhenius fit parameters (pre-exponential factor (D_0) and activation energy (E_A)) and coefficient of determinations (R^2) for D_{self} of H_2S in MEA/water solutions with different MEA concentrations. The values of D_{self} of H_2S were fitted for a temperature range of 293–353 K.

MEA concentration / [wt. %]	D_0 / [$\text{m}^2 \text{s}^{-1}$]	E_A / [kJ mol^{-1}]	R^2
10	8.41×10^{-7}	15.36	0.985
20	6.76×10^{-7}	15.31	0.985
30	9.84×10^{-7}	16.86	0.991
40	3.10×10^{-6}	21.61	0.991
50	3.48×10^{-6}	23.06	0.992

Fig. 4 shows RDFs of CO_2 and H_2S with water and MEA molecules as a function of the MEA concentration in MEA/water solutions. For the MEA concentrations, the peak positions of CO_2 -MEA and H_2S -MEA RDFs are similar. However, the results show that the intensity of the first peaks in CO_2 -MEA and H_2S -MEA RDFs increases with decreasing MEA concentration in the solution. These results indicate that acid gas-MEA interactions are stronger with respect to the decreasing MEA concentration in the solutions. In the CO_2 -water RDF, it can be observed that the first peak gets widened and more intense with increasing MEA concentration in the solution. In the H_2S -water RDF, the first peak positions do not change while the intensities of the first peak show a trend of decreasing with increasing MEA concentration in the solution. These results mainly indicate a weaker interaction between H_2S and water molecules with respect to the increase in the concentration of MEA in the solutions. The second peaks in H_2S -water RDFs slightly change position in the solutions with different MEA concentration. Intensities of the second peak in H_2S -water RDF also change with changing MEA concentration in the solution. The intensity decreases from 10 to 40 wt.% while it increases from 30 to 40 wt.%. Overall, our results show that the MEA concentration in aqueous MEA solutions significantly affects the acid gas-MEA and acid gas-water interactions. The RDFs we computed indicate that both acid gas-MEA interactions and acid gas-water interactions will become weaker with increasing MEA concentration in the solution. With weaker interactions with the surrounding molecules, we would expect that values of D_{self} of both acid gases increase with increasing MEA concentration. However, Fig. 3 shows that values of D_{self} decrease significantly with increasing MEA concentration in the solution. This is because of increased viscosity of the solution with increasing MEA concentration [65], i.e. values of D_{self} of every molecule type in the solution decrease (Fig. 3 and Fig. S4) with increasing MEA concentration.

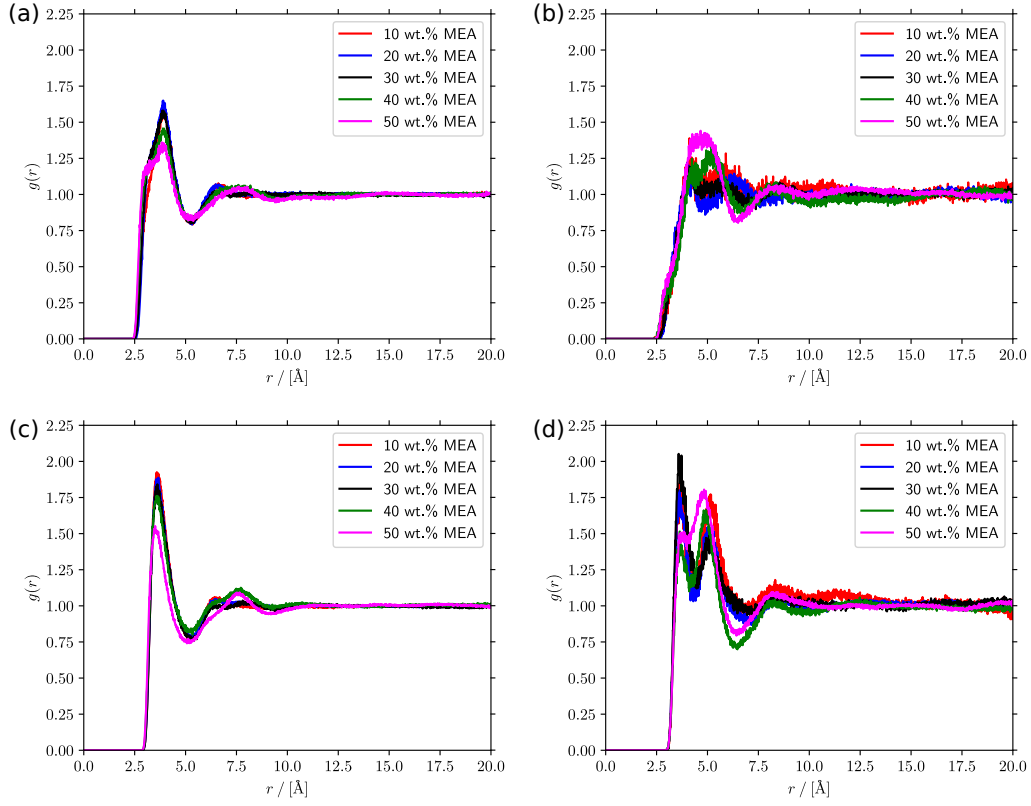


Figure 4: Radial distribution functions of (a) CO₂ -MEA, (b) CO₂ -water, (c) H₂S -MEA, and (d) H₂S -water for 10–50 wt.% MEA/water solutions at 293 K and 1 bar.

4. Conclusions

We investigated the effect of temperature and MEA concentration on the self-diffusivity of CO₂ and H₂S in aqueous MEA solutions. For this purpose, we computed densities of pure MEA and 30 wt.% MEA/water solutions as a function of temperature and the scaling factor for point charges of MEA (χ). We showed that scaling factor $\chi = 0.80$ can be used to obtain a good agreement between molecular simulations and experiments from literature. We validated this scaling factor by computing viscosities and self-diffusivity of pure MEA and 30 wt.% MEA/water solutions at 293–353 K. The scaling factor of $\chi = 0.80$ was validated by comparing the computed and experimental viscosities and the self-diffusivities of pure MEA and 30 wt.% MEA/water solutions. We computed the self-diffusivities of CO₂ and H₂S at infinite dilution, at 293–353 K and 1 bar, for 10–50 wt.% MEA/water solutions. The results showed that D_{self} of acid gases significantly depends on the MEA concentration in the solution. It is also shown that D_{self} of CO₂ is larger than D_{self} of H₂S despite molecular weight of CO₂ (44.01 g mol⁻¹) being higher than that of H₂S (34.1 g mol⁻¹).

Acknowledgement

This work was supported by the Carbon Capture Utilization and Storage R&D program from TotalEnergies S.E. This work has been financially supported by ANRT, CIFRE Convention no. 2019/0860. We are grateful for the support by NWO Domain Science for the use of supercomputer facilities, with financial support from the Nederlandse Organisatie voor Wetenschappelijk Onderzoek (Netherlands Organisation for Scientific Research, NWO). T.J.H.V. acknowledges NWO-CW (Chemical Sciences) for a VICI grant.

References

- [1] U.S. Energy Information Administration, , How much carbon dioxide is produced when different fuels are burned? (2021).
URL <https://www.eia.gov/tools/faqs/faq.php?id=73&t=11>
- [2] F.-Y. Liang, M. Ryvak, S. Sayeed, N. Zhao, The role of natural gas as a primary fuel in the near future, including comparisons of acquisition, transmission and waste handling costs of as with competitive alternatives, *Chemistry Central Journal* 6 (2012) S4. doi:10.1186/1752-153x-6-s1-s4.
- [3] U.S. Department of Energy, Alternative fuels price report, Tech. rep., U.S. Department of Energy (2021).
- [4] F. Holz, P. M. Richter, R. Egging, A global perspective on the future of natural gas: Resources, trade, and climate constraints, *Review of Environmental Economics and Policy* 9 (2015) 85–106. doi:10.1093/reep/reu016.
- [5] P. Theveneau, X. Xu, O. Baudouin, J. N. Jaubert, P. Ceragioli, C. Coquelet, Vapor-Liquid Equilibria of the $\text{CH}_4 + \text{CO}_2 + \text{H}_2\text{S}$ Ternary System with Two Different Global Compositions: Experiments and Modeling, *Journal of Chemical and Engineering Data* 65 (2020) 1802–1813. doi:10.1021/acs.jced.9b01082.
- [6] W. F. Burgers, P. S. Northrop, H. S. Kheshgi, J. A. Valencia, Worldwide development potential for sour gas, in: *Energy Procedia*, Vol. 4, Elsevier Ltd, 2011, pp. 2178–2184. doi:10.1016/j.egypro.2011.02.104.
- [7] V. Rozyyev, C. T. Yavuz, An All-Purpose Porous Cleaner for Acid Gas Removal and Dehydration of Natural Gas (11 2017). doi:10.1016/j.chempr.2017.10.014.
- [8] G. George, N. Bhorla, S. Alhallaq, A. Abdala, V. Mittal, Polymer membranes for acid gas removal from natural gas, *Separation and Purification Technology* 158 (2016) 333–356. doi:10.1016/j.seppur.2015.12.033.
- [9] X. Li, J. Li, B. Yang, Design and control of the cryogenic distillation process for purification of synthetic natural gas from methanation of coke oven gas, *Industrial and Engineering Chemistry Research* 53 (2014) 19583–19593. doi:10.1021/ie5024063.

- [10] J. S. Eow, Recovery of sulfur from sour acid gas: A review of the technology, *Environmental Progress* 21 (2002) 143–162. doi:10.1002/ep.670210312.
- [11] E. Skylogianni, I. Mundal, D. D. Pinto, C. Coquelet, H. K. Knuutila, Hydrogen sulfide solubility in 50 wt% and 70 wt% aqueous methyldiethanolamine at temperatures from 283 to 393 K and total pressures from 500 to 10000 kPa, *Fluid Phase Equilibria* 511 (2020). doi:10.1016/j.fluid.2020.112498.
- [12] S. Bishnoi, G. T. Rochelle, Absorption of carbon dioxide in aqueous piperazine/methyldiethanolamine, *AIChE Journal* 48 (2002) 2788–2799. doi:10.1002/aic.690481208.
- [13] M. Dicko, C. Coquelet, C. Jarne, S. Northrop, D. Richon, Acid gases partial pressures above a 50wt% aqueous methyldiethanolamine solution: Experimental work and modeling, *Fluid Phase Equilibria* 289 (2010) 99–109. doi:https://doi.org/10.1016/j.fluid.2009.11.012.
- [14] D. Y. C. Leung, G. Caramanna, M. Mercedes Maroto-Valer, An overview of current status of carbon dioxide capture and storage technologies, *Renewable and Sustainable Energy Reviews* 39 (2014) 426–443. doi:10.1016/j.rser.2014.07.093.
- [15] X. Rozanska, E. Wimmer, F. De Meyer, Quantitative Kinetic Model of CO₂ Absorption in Aqueous Tertiary Amine Solvents, *Journal of Chemical Information and Modeling* 61 (2021) 1814–1824. doi:10.1021/acs.jcim.0c01386.
- [16] A. A. Orlov, A. Valtz, C. Coquelet, X. Rozanska, E. Wimmer, G. Marcou, D. Horvath, B. Poulain, A. Varnek, Frédéric De Meyer, Computational screening methodology identifies effective solvents for CO₂ capture, *Communications Chemistry* 5 (2022) 1–7. doi:10.1038/s42004-022-00654-y.
- [17] S. Dara, A. S. Berrouk, Computer-based optimization of acid gas removal unit using modified CO₂ absorption kinetic models, *International Journal of Greenhouse Gas Control* 59 (2017) 172–183. doi:10.1016/J.IJGGC.2017.02.014.
- [18] H. A. Al-Ghawas, D. P. Hagewiesche, G. Ruiz-Ibanez, O. C. Sandall, Physicochemical Properties Important for Carbon Dioxide Absorption

- in Aqueous Methyldiethanolamine, *Journal of Chemical and Engineering Data* 34 (1989) 385–391. doi:10.1021/jc00058a004.
- [19] G. F. Versteeg, W. P. van Swaai, Solubility and diffusivity of acid gases (carbon dioxide, nitrous oxide) in aqueous alkanolamine solutions, *Journal of Chemical and Engineering Data* 33 (2002) 29–34. doi:10.1021/JE00051A011.
 - [20] Q. Chen, S. P. Balaji, M. Ramdin, J. J. Gutiérrez-Sevillano, A. Bardow, E. V. Goetheer, T. J. H. Vlucht, Validation of the CO₂/N₂O analogy using molecular simulation, *Industrial and Engineering Chemistry Research* 53 (2014) 18081–18090. doi:10.1021/ie503488n.
 - [21] M. Kohns, S. Werth, M. Horsch, E. von Harbou, H. Hasse, Molecular simulation study of the CO₂–N₂O analogy, *Fluid Phase Equilibria* 442 (2017) 44–52. doi:10.1016/j.fluid.2017.03.007.
 - [22] E. Sada, H. Kumazawa, M. A. Butt, Solubility and Diffusivity of Gases In Aqueous Solutions of Amines, *Journal of Chemical and Engineering Data* 23 (1978) 161–163. doi:10.1021/jc60077a008.
 - [23] J. J. Ko, T. C. Tsai, C. Y. Lin, H. M. Wang, M. H. Li, Diffusivity of nitrous oxide in aqueous alkanolamine solutions, *Journal of Chemical and Engineering Data* 46 (2001) 160–165. doi:10.1021/jc000138x.
 - [24] J. Ying, D. A. Eimer, Measurements and correlations of diffusivities of nitrous oxide and carbon dioxide in monoethanolamine + water by laminar liquid jet, *Industrial and Engineering Chemistry Research* 51 (2012) 16517–16524. doi:10.1021/ie302745d.
 - [25] R. V. Vaz, J. R. Gomes, C. M. Silva, Molecular dynamics simulation of diffusion coefficients and structural properties of ketones in supercritical CO₂ at infinite dilution, *Journal of Supercritical Fluids* 107 (2016) 630–638. doi:10.1016/j.supflu.2015.07.025.
 - [26] J. Wang, H. Zhong, H. Feng, W. Qiu, L. Chen, Molecular dynamics simulation of diffusion coefficients and structural properties of some alkylbenzenes in supercritical carbon dioxide at infinite dilution, *Journal of Chemical Physics* 140 (2014) 104501. doi:10.1063/1.4867274.

- [27] A. Tamimi, E. B. Rinker, O. C. Sandall, Diffusion Coefficients for Hydrogen Sulfide, Carbon Dioxide, and Nitrous Oxide in Water over the Temperature Range 293–368 K, *Journal of Chemical and Engineering Data* 39 (1994) 330–332. doi:10.1021/jc00014a031.
- [28] O. A. Moulτος, I. N. Tsimpanogiannis, A. Z. Panagiotopoulos, I. G. Economou, Atomistic molecular dynamics simulations of CO₂ diffusivity in H₂O for a wide range of temperatures and pressures, *Journal of Physical Chemistry B* 118 (2014) 5532–5541. doi:10.1021/jp502380r.
- [29] O. A. Moulτος, I. N. Tsimpanogiannis, A. Z. Panagiotopoulos, I. G. Economou, Self-diffusion coefficients of the binary (H₂O + CO₂) mixture at high temperatures and pressures, *Journal of Chemical Thermodynamics* 93 (2016) 424–429. doi:10.1016/j.jct.2015.04.007.
- [30] S. M. Melnikov, M. Stein, The effect of CO₂ loading on alkanolamine absorbents in aqueous solutions, *Physical Chemistry Chemical Physics* 21 (2019) 18386–18392. doi:10.1039/c9cp03976g.
- [31] S. Y. Oh, M. Binns, H. Cho, J. K. Kim, Energy minimization of mea-based CO₂ capture process, *Applied Energy* 169 (2016) 353–362. doi:10.1016/j.apenergy.2016.02.046.
- [32] T. L. S nderby, K. B. Carlsen, P. L. Fosb l, L. G. Ki rboe, N. von Solms, A new pilot absorber for CO₂ capture from flue gases: Measuring and modelling capture with mea solution, *International Journal of Greenhouse Gas Control* 12 (2013) 181–192. doi:10.1016/j.ijggc.2012.10.010.
- [33] R. Hens, A. Rahbari, S. Caro-Ortiz, N. Dawass, M. Erd s, A. Pour-saeidesfahani, H. S. Salehi, A. T. Celebi, M. Ramdin, O. A. Moulτος, D. Dubbeldam, T. J. H. Vlught, Brick-CFCMC: Open Source Software for Monte Carlo Simulations of Phase and Reaction Equilibria Using the Continuous Fractional Component Method, *Journal of Chemical Information and Modeling* 60 (2020) 2678–2682. doi:10.1021/acs.jcim.0c00334.
- [34] A. Rahbari, R. Hens, M. Ramdin, O. A. Moulτος, D. Dubbeldam, T. J. H. Vlught, Recent advances in the continuous fractional component Monte Carlo methodology, *Molecular Simulation* (2021) 804–823.
- [35] H. M. Polat, H. S. Salehi, R. Hens, D. O. Wasik, A. Rahbari, F. De Meyer, C. Houriez, C. Coquelet, S. Calero, D. Dubbeldam, O. A. Moulτος,

- T. J. H. Vlucht, New Features of the Open Source Monte Carlo Software Brick-CFCMC: Thermodynamic Integration and Hybrid Trial Moves, *Journal of Chemical Information and Modeling* 61 (2021) 3752–3757. doi:10.1021/acs.jcim.1c00652.
- [36] W. L. Jorgensen, D. S. Maxwell, J. Tirado-Rives, Development and testing of the opls all-atom force field on conformational energetics and properties of organic liquids, *Journal of the American Chemical Society* 118 (1996) 11225–11236. doi:10.1021/ja9621760.
- [37] R. C. Rizzo, W. L. Jorgensen, OPLS all-atom model for amines: Resolution of the amine hydration problem, *Journal of the American Chemical Society* 121 (1999) 4827–4836. doi:10.1021/ja984106u.
- [38] M. J. Frisch, G. W. Trucks, H. B. Schlegel, G. E. Scuseria, M. A. Robb, J. R. Cheeseman, G. Scalmani, V. Barone, B. Mennucci, G. A. Petersson, H. Nakatsuji, M. Caricato, X. Li, H. P. Hratchian, A. F. Izmaylov, J. Bloino, G. Zheng, J. L. Sonnenberg, M. Hada, M. Ehara, K. Toyota, R. Fukuda, J. Hasegawa, M. Ishida, T. Nakajima, Y. Honda, O. Kitao, H. Nakai, T. Vreven, J. A. Montgomery, Jr., J. E. Peralta, F. Ogliaro, M. Bearpark, J. J. Heyd, E. Brothers, K. N. Kudin, V. N. Staroverov, R. Kobayashi, J. Normand, K. Raghavachari, A. Rendell, J. C. Burant, S. S. Iyengar, J. Tomasi, M. Cossi, N. Rega, J. M. Millam, M. Klene, J. E. Knox, J. B. Cross, V. Bakken, C. Adamo, J. Jaramillo, R. Gomperts, R. E. Stratmann, O. Yazyev, A. J. Austin, R. Cammi, C. Pomelli, J. W. Ochterski, R. L. Martin, K. Morokuma, V. G. Zakrzewski, G. A. Voth, P. Salvador, J. J. Dannenberg, S. Dapprich, A. D. Daniels, O. Farkas, J. B. Foresman, J. V. Ortiz, J. Cioslowski, D. J. Fox, *Gaussian 09 Revision E.01*, gaussian Inc. Wallingford CT 2009 (2016).
- [39] C. Møller, M. S. Plesset, Note on an approximation treatment for many-electron systems, *Physical Review* 46 (1934) 618–622. doi:10.1103/PhysRev.46.618.
- [40] H. J. C. Berendsen, J. R. Grigera, T. P. Straatsma, The missing term in effective pair potentials, *The Journal of Physical Chemistry* 91 (1987) 6269–6271. doi:10.1021/j100308a038.
- [41] I. N. Tsimpanogiannis, O. A. Moulτος, L. F. Franco, M. B. M. Spera, M. Erdős, I. G. Economou, Self-diffusion coefficient of bulk and confined

- water: a critical review of classical molecular simulation studies, *Molecular Simulation* 45 (2019) 425–453. doi:10.1080/08927022.2018.1511903.
- [42] J. J. Potoff, J. I. Siepmann, Vapor–liquid equilibria of mixtures containing alkanes, carbon dioxide, and nitrogen, *AIChE Journal* 47 (2001) 1676–1682. doi:10.1002/aic.690470719.
 - [43] G. A. Orozco, V. Lachet, C. Nieto-Draghi, A. D. MacKie, A transferable force field for primary, secondary, and tertiary alkanolamines, *Journal of Chemical Theory and Computation* 9 (2013) 2097–2103.
URL <https://pubs.acs.org/doi/full/10.1021/ct301098s>
 - [44] T. Kristóf, J. Liszi, Effective Intermolecular Potential for Fluid Hydrogen Sulfide, *The Journal of Physical Chemistry B* 101 (1997) 5480–5483. doi:10.1021/jp9707495.
 - [45] M. P. Allen, D. J. Tildesley, *Computer Simulation of Liquids*, 2nd Edition, Oxford University Press, Oxford, UK, 2017.
 - [46] L. Martinez, R. Andrade, E. G. Birgin, J. M. Martínez, PACKMOL: A package for building initial configurations for molecular dynamics simulations, *Journal of Computational Chemistry* 30 (2009) 2157–2164. doi:10.1002/jcc.21224.
 - [47] P. P. Ewald, Die Berechnung optischer und elektrostatischer Gitterpotentiale, *Annalen der Physik* 369 (1921) 253–287. doi:10.1002/andp.19213690304.
 - [48] S. Plimpton, Fast Parallel Algorithms for Short-Range Molecular Dynamics, *Journal of Computational Physics* 117 (1995) 1–19. doi:<https://doi.org/10.1006/jcph.1995.1039>.
 - [49] S. H. Jamali, L. Wolff, T. M. Becker, M. de Groen, M. Ramdin, R. Hartkamp, A. Bardow, T. J. H. Vlugt, O. A. Moultos, OCTP: A Tool for On-the-Fly Calculation of Transport Properties of Fluids with the Order-n Algorithm in LAMMPS, *Journal of Chemical Information and Modeling* 59 (2019) 1290–1294. doi:10.1021/acs.jcim.8b00939.
 - [50] S. H. Jamali, L. Wolff, T. M. Becker, A. Bardow, T. J. H. Vlugt, O. A. Moultos, Finite-Size Effects of Binary Mutual Diffusion Coefficients from

- Molecular Dynamics, *Journal of Chemical Theory and Computation* 14 (2018) 2667–2677. doi:10.1021/acs.jctc.8b00170.
- [51] A. T. Celebi, S. H. Jamali, A. Bardow, T. J. H. Vlugt, O. A. Moulton, Finite-size effects of diffusion coefficients computed from molecular dynamics: a review of what we have learned so far, *Molecular Simulation* 47 (2021) 831–845. doi:10.1080/08927022.2020.1810685.
 - [52] S. H. Jamali, A. Bardow, T. J. H. Vlugt, O. A. Moulton, Generalized Form for Finite-Size Corrections in Mutual Diffusion Coefficients of Multicomponent Mixtures Obtained from Equilibrium Molecular Dynamics Simulation, *Journal of Chemical Theory and Computation* 16 (2020) 3799–3806. doi:10.1021/acs.jctc.0c00268.
 - [53] R. Krishna, J. A. Wesselingh, The Maxwell-Stefan approach to mass transfer, *Chemical Engineering Science* 52 (1997) 861–911. doi:10.1016/S0009-2509(96)00458-7.
 - [54] A. T. Celebi, N. Dawass, O. A. Moulton, T. J. H. Vlugt, How sensitive are physical properties of choline chloride-urea mixtures to composition changes: Molecular dynamics simulations and Kirkwood-Buff theory, *Journal of Chemical Physics* 154 (2021) 184502. doi:10.1063/5.0049064.
 - [55] A. Chaumont, E. Engler, R. Schurhammer, Is Charge Scaling Really Mandatory when Developing Fixed-Charge Atomistic Force Fields for Deep Eutectic Solvents?, *Journal of Physical Chemistry B* 124 (2020) 7239–7250. doi:10.1021/acs.jpcc.0c04907.
 - [56] A. González De Castilla, J. P. Bittner, S. Müller, S. Jakobtorweihen, I. Smirnova, Thermodynamic and Transport Properties Modeling of Deep Eutectic Solvents: A Review on gE-Models, Equations of State, and Molecular Dynamics, *Journal of Chemical and Engineering Data* 65 (2020) 943–967. doi:10.1021/acs.jced.9b00548.
 - [57] V. V. Chaban, I. V. Voroshylova, O. N. Kalugin, A new force field model for the simulation of transport properties of imidazolium-based ionic liquids, *Physical Chemistry Chemical Physics* 13 (2011) 7910–7920. doi:10.1039/c0cp02778b.
 - [58] S. Blazquez, I. M. Zeron, M. M. Conde, J. L. Abascal, C. Vega, Scaled charges at work: Salting out and interfacial tension of methane with

- electrolyte solutions from computer simulations, *Fluid Phase Equilibria* 513 (2020) 112548. doi:10.1016/j.fluid.2020.112548.
- [59] I. M. Zeron, J. L. Abascal, C. Vega, A force field of Li^+ , Na^+ , K^+ , Mg^{2+} , Ca^{2+} , Cl^- , and SO_4^{2-} in aqueous solution based on the TIP4P/2005 water model and scaled charges for the ions, *Journal of Chemical Physics* 151 (2019) 134504. doi:10.1063/1.5121392.
 - [60] H. Liu, E. Maginn, A. E. Visser, N. J. Bridges, E. B. Fox, Thermal and transport properties of six ionic liquids: An experimental and molecular dynamics study, *Industrial and Engineering Chemistry Research* 51 (2012) 7242–7254. doi:10.1021/ie300222a.
 - [61] S. L. Perkins, P. Painter, C. M. Colina, Molecular dynamic simulations and vibrational analysis of an ionic liquid analogue, *Journal of Physical Chemistry B* 117 (2013) 10250–10260. doi:10.1021/jp404619x.
 - [62] S. L. Perkins, P. Painter, C. M. Colina, Experimental and computational studies of choline chloride-based deep eutectic solvents, *Journal of Chemical and Engineering Data* 59 (2014) 3652–3662. doi:10.1021/je500520h.
 - [63] T. G. Amundsen, L. E. Øi, D. A. Eimer, Density and viscosity of monoethanolamine + water + carbon dioxide from (25 to 80) °C, *Journal of Chemical and Engineering Data* 54 (2009) 3096–3100. doi:10.1021/je900188m.
 - [64] W. V. Wilding, T. A. Knotts, N. F. Giles, R. L. Rowley, DIPPR® Data Compilation of Pure Chemical Properties, AIChE, New York, NY, 2020.
 - [65] M. Sobrino, E. I. Concepción, Á. Gómez-Hernández, M. C. Martín, J. J. Segovia, Viscosity and density measurements of aqueous amines at high pressures: Mdea-water and mea-water mixtures for CO_2 capture, *Journal of Chemical Thermodynamics* 98 (2016) 231–241. doi:10.1016/j.jct.2016.03.021.
 - [66] G. T. Rochelle, Conventional amine scrubbing for CO_2 capture, *Absorption-Based Post-Combustion Capture of Carbon Dioxide* (2016) 35–67.
 - [67] H. M. Polat, M. Zeeshan, A. Uzun, S. Keskin, Unlocking CO_2 separation performance of ionic liquid/cubtc composites: Combining experiments

- with molecular simulations, *Chemical Engineering Journal* 373 (2019) 1179–1189. doi:10.1016/j.cej.2019.05.113.
- [68] M. N. Rodnikova, F. M. Samigullin, I. A. Solonina, D. A. Sirotkin, Molecular mobility and the structure of polar liquids, *Journal of Structural Chemistry* 55 (2014) 256–262. doi:10.1134/S0022476614020097.
 - [69] M. N. Rodnikova, Z. S. Idiyatullin, I. A. Solonina, D. A. Sirotkin, A. B. Razumova, Molecular Self-Diffusion Coefficients in Solutions of Dimethylsulfoxide in Monoethanolamine, *Russian Journal of Physical Chemistry A* 92 (2018) 1486–1488. doi:10.1134/S0036024418080198.
 - [70] B. P. Mandal, M. Kundu, S. S. Bandyopadhyay, Physical solubility and diffusivity of n₂o and co₂ into aqueous solutions of (2-amino-2-methyl-1-propanol + monoethanolamine) and (n-methyldiethanolamine + monoethanolamine), *Journal of Chemical and Engineering Data* 50 (2005) 352–358.
 - [71] T. C. Chan, H. T. Li, K. Y. Li, Effects of Shapes of Solute Molecules on Diffusion: A Study of Dependences on Solute Size, Solvent, and Temperature, *Journal of Physical Chemistry B* 119 (2015) 15718–15728. doi:10.1021/acs.jpcb.5b10550.
 - [72] R. J. Speedy, C. A. Angell, Isothermal compressibility of supercooled water and evidence for a thermodynamic singularity at -45°C, *The Journal of Chemical Physics* 65 (1976) 851–858. doi:10.1063/1.433153.
 - [73] W. Lu, H. Guo, I. M. Chou, R. C. Burruss, L. Li, Determination of diffusion coefficients of carbon dioxide in water between 268 and 473K in a high-pressure capillary optical cell with in situ Raman spectroscopic measurements, *Geochimica et Cosmochimica Acta* 115 (2013) 183–204.